



Contents lists available at ScienceDirect

Engineering

journal homepage: www.elsevier.com/locate/eng

Research
Electrical and Electronic Engineering—Article

Droplet-Enabled Controllable Manipulation of Ribo-Charges from Liquid-Solid Interface

Xunjia Li ^{a,b,c}, Jianjun Luo ^{b,d,*}, Jianfeng Ping ^{a,c,*}, Zhong Lin Wang ^{b,e,*}

^a College of Biosystems Engineering and Food Science, Zhejiang University, Hangzhou 310058, China

^b CAS Center for Excellence in Nanoscience, Beijing Institute of Nanoenergy and Nanosystems, Chinese Academy of Sciences, Beijing 101400, China

^c Innovation Platform of Micro/Nano Technology for Biosensing, ZJU-Hangzhou Global Scientific and Technological Innovation Center, Zhejiang University, Hangzhou 311215, China

^d School of Nanoscience and Engineering, University of Chinese Academy of Sciences, Beijing 100049, China

^e Yonsei Frontier Lab, Yonsei University, Seoul 03722, Republic of Korea

ARTICLE INFO

Article history:

Received 19 February 2024

Revised 17 April 2024

Accepted 8 July 2024

Available online 2 August 2024

Keywords:

Solid–liquid interface engineering

Energy harvesting device

Triboelectric nanogenerator

Interface charge utilization

Water energy

ABSTRACT

Efficient utilization of electrostatic charges is paramount for numerous applications, from printing to kinetic energy harvesting. However, existing technologies predominantly focus on the static qualities of these charges, neglecting their dynamic capabilities as carriers for energy conversion. Herein, we report a paradigm-shifting strategy that orchestrates the swift transit of surface charges, generated through contact electrification, via a freely moving droplet. This technique ingeniously creates a bespoke charged surface which, in tandem with a droplet acting as a transfer medium to the ground, facilitates targeted charge displacement and amplifies electrical energy collection. The spontaneously generated electric field between the charged surface and needle tip, along with the enhanced water ionization under the electric field, proves pivotal in facilitating controlled charge transfer. By coupling the effects of charge self-transfer, contact electrification, and electrostatic induction, a dual-electrode droplet-driven-triboelectric nanogenerator (DD–TENG) is designed to harvest the water-related energy, exhibiting a two-order-of-magnitude improvement in electrical output compared to traditional single-electrode systems. Our strategy establishes a fundamental groundwork for efficient water drop energy acquisition, offering deep insights and substantial utility for future interdisciplinary research and applications in energy science.

© 2024 THE AUTHORS. Published by Elsevier LTD on behalf of Chinese Academy of Engineering and Higher Education Press Limited Company. This is an open access article under the CC BY-NC-ND license (<http://creativecommons.org/licenses/by-nc-nd/4.0/>).

1. Introduction

Electrostatic charge arise from the redistribution of electrons at the atomic level, constituting the cornerstone of physical phenomena with far-reaching effects [1,2]. The application of electrostatic charges spans various industries and scientific disciplines, emphasizing their indispensable role in the progress of modern technology [3,4]. In the industrial sector, electrostatic coating techniques leverage the inherent electrical properties of materials to achieve precise and uniform coverage, enhancing the adhesion and durability of coatings [5,6]. In the field of healthcare, electrophoretic separation methods, driven by electric forces, enable the precise analysis and isolation of biomolecules [7,8]. In the energy sector, triboelectric nanogenerators (TENGs), based on the principles of

contact electrification and electrostatic induction, efficiently capture and convert mechanical energy from the environment, heralding a new era of green energy [9,10]. From a theoretical standpoint, practices ranging from printing to microenergy harvesting primarily rely on harnessing the static attributes of electrostatic charges, largely neglecting the exploration of their dynamic properties.

Meanwhile, a unique correlation between electrostatic charges and water has emerged. Recent research has revealed that the generation of electrostatic charges can be achieved through the contact of water droplets with a polymer surface. This phenomenon has been confirmed to be associated with the formation of a dynamic electric double layer (EDL) and charge transfer at the solid–liquid interface during the contact process, giving rise to various new applications, including the water droplet-driven TENGs [11–14]. However, droplet-driven TENGs are still limited to the utilization of tribo-charges (mostly electrons) based on the electrostatic induction effect at the water-polymer interface. This neglects the dynamic nature of charges as carriers and the

* Corresponding authors.

E-mail addresses: luojianjun@binn.cas.cn (J. Luo), jfping@zju.edu.cn (J. Ping), zhong.wang@mse.gatech.edu (Z.L. Wang).

<https://doi.org/10.1016/j.eng.2024.07.013>

2095-8099/© 2024 THE AUTHORS. Published by Elsevier LTD on behalf of Chinese Academy of Engineering and Higher Education Press Limited Company.

This is an open access article under the CC BY-NC-ND license (<http://creativecommons.org/licenses/by-nc-nd/4.0/>).

resulting opportunities for energy harvesting, preventing droplet-driven TENGs from achieving similar output performance as solid–solid TENGs. How to utilize the dynamic properties of charges to improved energy conversion efficiency of droplet-driven TENGs? The phenomenon of the floating water bridge, stemming from the Taylor cone, offers us a new perspective [15,16]. It not only underscores the influence of water as a medium on electric field distribution but also demonstrates the potential of water as a channel for charge transfer. Hence, a comprehensive grasp of charge transfer at solid–liquid interfaces is crucial to maximizing the capabilities of TENGs and related electrostatic technologies, propelling energy harvesting advancements and enhancing the influence of electrostatics in tech innovation.

In this paper, we propose a strategy for controllable charged surface construction and directional tribo-charge (electron) transfer via water. By adjusting droplet characteristics in liquid–solid contact electrification, controllable surface charge regions can be precisely generated. Subsequently, spontaneous and directed transfer of surface electrostatic charges is achieved using a water droplet as the transfer medium, along with the harvesting of accompanying energy. The mechanism of controllable charge transfer at the solid–liquid interface is also studied, which is associated with the induced spontaneous electric field, as well as the enhanced ionization of water molecules. Moreover, by combining the static and dynamic properties of tribo-charges, a dual-electrode droplet-driven (DD) triboelectric nanogenerator (TENG) is designed to harvest water droplet energy. Compared to traditional single-electrode droplet-driven (SD)–TENG, the DD–TENG exhibits significant advantages in enhancing charge utilization efficiency and electrical output, demonstrating its tremendous potential in energy harvesting applications.

2. Materials and methods

2.1. Chemicals

Unless otherwise specified, deionized (DI) water with a resistivity of $18.3 \text{ M}\Omega\text{-cm}^{-1}$ was employed for measurements. The following chemicals were procured from Sigma Aldrich (USA): NaCl ($\geq 99\%$), ethanol ($\geq 99.5\%$), octadecane ($\geq 95\%$), acetone ($\geq 99.5\%$), acetonitrile ($\geq 99.7\%$), methanol ($\geq 99.7\%$), glycerol ($\geq 99\%$), toluene ($\geq 99.5\%$), and paraffin wax and HCl (36.0%–38.0%), NaOH ($\geq 96.0\%$), acetic acid, sodium sulfate ($\geq 99.0\%$), dichloromethane ($\geq 99.5\%$), sodium sulfate ($\geq 98.0\%$), sodium carbonate ($\geq 99.8\%$), calcium chloride ($\geq 96.0\%$), sulfuric acid (95.0%–98.0%), and *n*-hexane ($\geq 95\%$) were sourced from China National Pharmaceutical Group Chemical Reagent Co., Ltd., China Polydimethylsiloxane (PDMS) precursor and curing agent were acquired from Corning Incorporated, USA.

2.2. Contact surface preparation

A laser cutting method was employed to create a $14 \text{ cm} \times 5 \text{ cm}$ dimension polymethyl methacrylate (PMMA) sheet, serving as a substrate to support the polytetrafluoroethylene (PTFE) film (Chukoh FLO, Japan). Dual-sided copper foil tape with dimensions of $5 \text{ cm} \times 5 \text{ cm}$ acted as the bottom electrode and affixed to the PMMA sheet surface. Conductive wires were then extended from the edge of copper tape, and a flexible scraper was utilized to flatten the tape. Following this, a PTFE film measuring $10 \text{ cm} \times 10 \text{ cm}$ was cut and placed over the copper electrode, enveloping the PMMA sheet. The entire assembly was introduced into a vacuum drying chamber to remove any trapped air bubbles, thereby ensuring a smooth and even PTFE surface.

2.3. Charging region generation

The PTFE surface, affixed onto a PMMA base, was positioned at a 30° angle relative to the ground. A stainless steel needle connected to an injection pump generated DI water droplets with a volume of approximately $35 \mu\text{L}$, which continuously impacted the PTFE surface center. The droplets were released at a rate of approximately 1 droplet per second. The adjustment of the charging region area and charge density was achieved by controlling the impact height and frequency. The spreading and retraction dynamics of water droplets were captured using a high-speed camera (Photron, FASTCAM Mini A, Japan) at a recording speed of 2000 frames per second (fps). The needle was grounded to prevent droplet charging by contact with the infusion tube wall. In typical measurements, ambient temperature was maintained at 25°C and relative humidity controlled within the range of 40% to 50%.

2.4. Spontaneous deformation of the droplet

The pre-charged PTFE surface was fixed parallel to the ground, and a droplet was deposited in the center of the charged region using a micropipette. A stainless steel pinhead (1 mm in diameter and 5 cm in length) connected to ground or electrometer's probe was affixed at the top of a vertically adjustable cantilever. The pinhead tip was positioned directly above the water droplet on charged surface, and the bottom electrode was also grounded. By programming, the cantilever was controlled to move the needle tip up and down within a defined range, facilitating contact and separation between the needle tip and the droplet. The dynamics of water droplets was recording using a high-speed camera at a typical recording speed of 2000 fps. In typical measurements, ambient temperature was maintained around 25°C and relative humidity controlled within the range of 40% to 50%.

2.5. Fabrication of DD–TENG

DD–TENG was designed on the basis of contact surface. To construct the upper electrode, we assembled a tiny conductive copper tape of size of $1 \text{ mm} \times 30 \text{ mm} \times 30 \mu\text{m}$ onto the as-prepared PTFE film surface. For comparison, an SD–TENG was manufactured in a similar manner, albeit without the upper electrode. The dynamics of water droplets was recording using a high-speed camera at a typical recording speed of 2000 fps. In typical measurements, ambient temperature was maintained around 25°C and relative humidity controlled within the range of 40% to 50%.

2.6. Electrical measurement

During the process of surface charge generation, a DI water droplet of $35 \mu\text{L}$ impacts the PTFE surface and subsequently rebounds into a Faraday cup. The charge carried by each droplet is recorded. The bottom electrode was connected to an electrometer (Keithley 6514, USA), which synchronously measures the charge generated on the PTFE surface during the impact process based on the principle of electrostatic induction. The surface potential of the impact location is measured using an electrostatic voltmeter with a non-contact probe (TREK, Model 347, USA). The probe was fixed on an XY-axis displacement stage, allowing continuous scanning of the PTFE surface according to a programmed path. By combining the coordinates, the distribution of surface potential on the PTFE surface can be obtained. An ion blower was used to blow the PTFE surface for approximately 10 s before each new experiment to eliminate excess charges.

During contact with the water droplet on charged surface, the grounded pinhead was connected to the ground through an

electrometer, which is used to record the transferred charge amount. Simultaneously, the bottom electrode is connected to another electrometer, which measured the variation in charge on the PTFE surface during the impact process based on the principle of electrostatic induction.

We employed an oscilloscope (Tektronix, MDO3000, USA) equipped with high-impedance (100 M Ω) probes to measure the voltage output of the DD-TENG and SD-TENG. The current and charge transfer between the bottom and upper electrodes were measured using an electrometer and a Faraday cup, respectively. The testing of transferred charge as a function of the Weber number or the variation in the maximum spreading area was achieved by altering the droplet release height. For typical measurements, we maintained the relative humidity at approximately 65.0% and the ambient temperature at 20.0 $^{\circ}$ C, respectively.

2.7. Calculation methods

2.7.1. Calculation of surface charge density

We calculated the distribution of charge on the PTFE surface based on the surface potential data. The surface charge density on PTFE surface σ can be converted by the surface potential V [17]:

$$\sigma = \frac{\epsilon_0 \epsilon_r V}{d}$$

Where ϵ_0 is the vacuum dielectric constant, ϵ_r is the relative dielectric constant of the PTFE film, and d represents the thickness of the PTFE film.

2.7.2. Calculation of energy conversion efficiency

For energy harvesting devices, the most crucial aspect is to characterize their output power and energy conversion efficiency. By connecting different load resistors in the external circuit, the output voltage of the DD-TENG was tested, and the instantaneous output power P of the DD-TENG under different loads was calculated:

$$P = \frac{U^2}{RS}$$

Where U is the voltage across the load resistor, R is the value of the load resistor, and S is the maximum spreading area of the water droplet. Subsequently, the energy output E_{out} per water droplet under different loads was calculated:

$$E_{\text{out}} = \int \frac{U^2}{Rdt}$$

Since the water droplet's impact height is relatively low and the resistance it encounters can be neglected, the energy carried by each water droplet upon impact due to gravity E_{in} can be expressed as:

$$E_{\text{in}} = mgh$$

Where m is the mass of the water droplet, h is the height from which the water droplet falls, and g is the gravitational acceleration. Therefore, the energy conversion efficiency η of the DD-TENG for each water droplet can be expressed as:

$$\eta = \frac{E_{\text{out}}}{E_{\text{in}}}$$

Additionally, the calculated energy conversion efficiency is lower than the actual efficiency due to the omission of energy losses from friction, residual kinetic energy, and dissipation during the calculations.

3. Results and discussions

3.1. Spontaneous transfer of liquid–solid contact-induced tribo-charges

We observed spontaneous morphological changes in the droplet when a grounded needle tip touched a free droplet of 10 μ L deposited on a surface charged by liquid–solid contact (Fig. 1(a) and Movie S1 in Appendix A). In comparison, the droplet on the uncharged surface exhibited no change before and after needle contact (Fig. S1 and Movie S2 in Appendix A), implying that surface charges are the critical factor in causing this difference. This phenomenon resembles the change in contact angle of droplets governed by an external electric field in electrowetting-on-dielectric (EWOD). However, morphological changes of droplets in EWOD require the application of an electric potential to the microelectrode array to control the wetting characteristics of droplets on the dielectric film [18,19]. In contrast, this spontaneous morphological transformation occurs without external power interference. The generation of an direct current (DC) signal accompanies this transformation. When touching the water droplet on the charged surface with a needle tip, the instantaneous DC output can reach 250 V (Fig. 1(b)) and 50 nC (Fig. S2(a) in Appendix A), respectively, while no output signal can be observed for the uncharged surface. This instantaneous energy can light up \sim 230 light-emitting diodes (LEDs; Fig. S2(b) in Appendix A). In addition, the potential around the droplet location on the charged surface is significantly lower after contact with the grounding tip (Fig. 1(c)) compared to the initial state (Fig. S3 in Appendix A). As the surface potential is proportional to the charge density [17], this result indicates a noteworthy decline in the charge density within the droplet-located region.

How do these phenomena occur without any external electric field? We propose that these occurrences are caused by a rapid to ground release of surface tribo-charges from the region covered by the water droplet as a conduction channel (Fig. 1(d)). This is different from the previous conventional understanding that the surface charges caused by liquid–solid contact are stable and can even be used for spontaneous droplet transport or energy collection [20–22]. The phenomenon of spontaneous charge transfer indicates that the tribo-charge generated by contact electrification can be controllably removed or utilized. Our study indicates the tribo-charges in this case are mostly electrons, which can be conducted away through the contacting tip.

3.2. Construction of controllable charged surface

To verify the reproducibility of the above-mentioned phenomenon, we propose a surface charge printing strategy based on liquid–solid contact initiation that can be used to form controllable surface charge distribution regions. PTFE, a common electronegative material, was chosen as a solid contact substrate, and water droplets were released at a fixed height. In this process, the surface charges are generated at the impact area on PTFE due to contact electrification at the liquid–solid interface (Fig. 2(a)), as contributed mostly by transferred electrons. When water droplets impact the PTFE surface, a rapid deformation ensues, accompanied by the charge separation due to contact electrification (Fig. S4 in Appendix A). The Weber number, which represents the ratio of inertial forces to surface tension effects, is introduced to analyze the motion state of water droplets. Electrometer measurements reveal a rise in the charge amount on the PTFE surface with increasing Weber number (Fig. 2(b)). Since the droplet's impact velocity and coverage area will increase with drop height, there is a positive relationship between the surface charge amount and the Weber number (Fig. S5 in Appendix A). Similar rules emerge from the surface potential scan results (Fig. S6 in Appendix A).

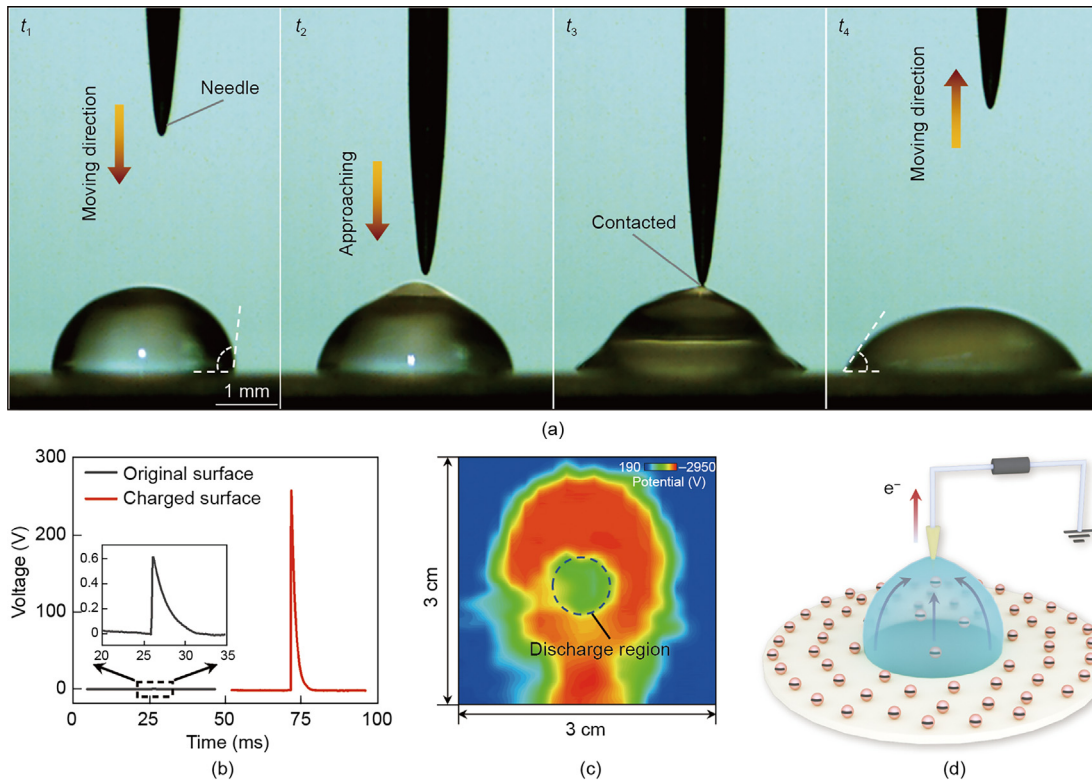


Fig. 1. Water droplet induced surface charge spontaneous transfer. (a) Morphological changes of the water droplet on a charged surface as the grounded needle tip approaches. The changes in liquid contact angle before and after releasing the charge indicate the electron transfers through the liquid to the tip t_1 – t_4 : time. (b) Charge transfer signals generated when the grounded needle tip contacts the water droplets on charged and uncharged surfaces. (c) Potential distribution on the charged surface after the grounded needle contacts the water droplet. (a–c) The volume of water droplets was fixed at $\sim 10 \mu\text{L}$. (d) Schematic of spontaneous transfer of tribo-charges from the polytetrafluoroethylene (PTFE) surface through the droplets.

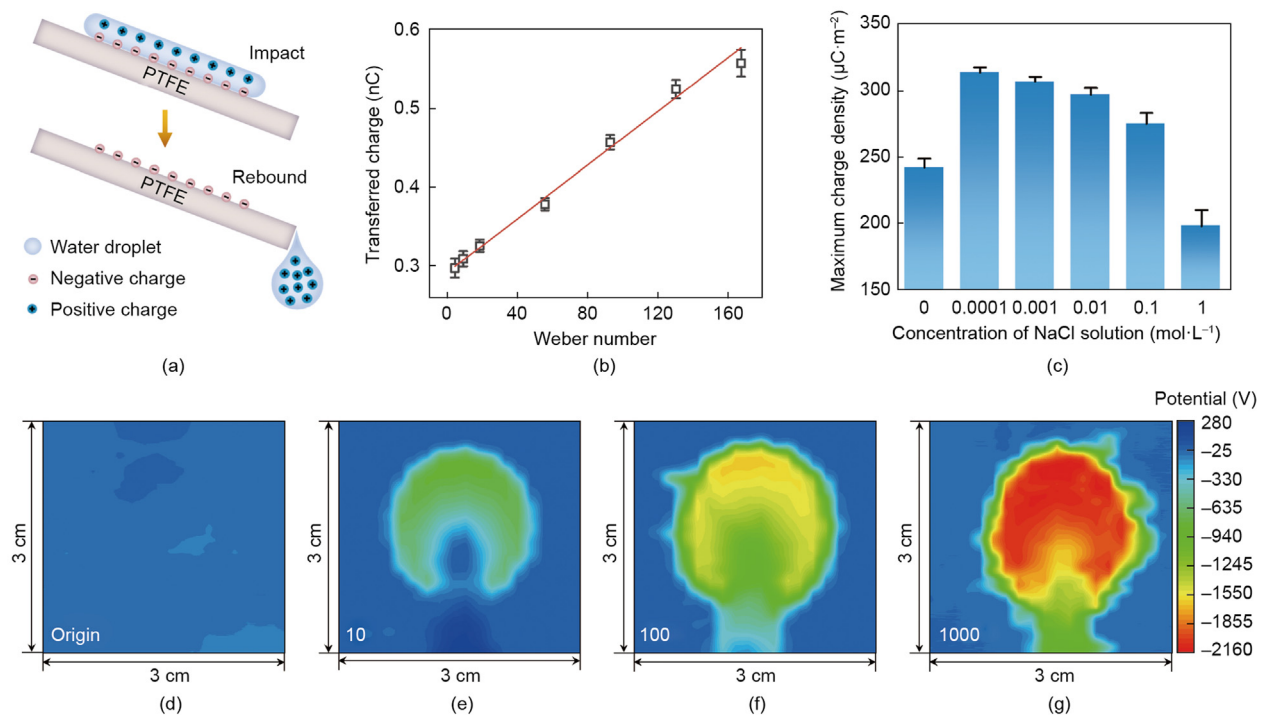


Fig. 2. Controllable charged surface construction through liquid–solid contact electrification. (a) Schematic diagram of tribo-charge generation process at the water droplet-PTFE contact interface. (b) Effect of the Weber number on the tribo-charge amount at the water droplet-PTFE contact interface. (c) Effect of NaCl concentration on the tribo-charge density on the PTFE surface. (d–g) Effect of water droplet impact number on surface potential distribution.

The contact electrification mechanism between water droplets and PTFE might involve both electron and ion transfers [23,24], rendering the charge generation efficiency of liquid–solid contact electrification particularly sensitive to the ion concentration of the liquid [25,26]. As depicted in Fig. 2(c), the electrification effect of NaCl solution enhances with increasing concentration in the low concentration interval (ranging from 0 to 0.0001 mol L⁻¹) due to the low ion concentration increases the proportion of ion transfer during contact (Fig. 2(c) and Fig. S7 in Appendix A) [27]. A significant decrease of maximum surface charge density is observed at a NaCl concentration of 1 mol L⁻¹, which may be attributed to the shielding effect of the high ion concentration weakening the charging ability of the liquid [23]. Similarly, the general trend indicates that the charge generated is greater when the pH is closer to neutral (Fig. S8(a) in Appendix A). In addition, organic reagents like ethanol and hexane exhibit a significantly reduced electrification effect when in contact with the PTFE surface (Fig. S8(b)). The influence of solid contact materials on contact electrification also deserves attention. As demonstrated in Fig. S9(a) (Appendix A), the quantity of transferred charges upon contact correlates with the density and type of strong electron-absorbing groups present in the solid material [28,29]. The equality of charges between the PTFE surface and water droplets is disrupted as the PTFE thickness increases, attributed to the influence of PTFE thickness on electrostatic induction in Fig. S9(b). The presence of the lower electrode does not affect tribo-charge generation (Fig. S10(a) in Appendix A), but grounding it strengthens induced charges within the electrode in Figs. S10(b)–(d), counteracting the initial electric field and promoting interface charge separation [20].

On the basis of the aforementioned experiments, we programmed the printing of the PTFE surface charge density by fixing the Weber number and varying the impact number of water droplet. As depicted in Figs. 2(d)–(g), the surface potential of PTFE continuously rises with an increasing number of droplet impacts, owing to the accumulation effect of tribo-charges. This effect is fre-

quently found in TENG-related researches and is connected with the electrical output of TENG [11,21,30]. Through continuous monitoring of the charges carried by water droplets, it was observed that, as the number of impacts increased, the charge carried by the droplets gradually decreased (Fig. S11(a) in Appendix A). This phenomenon can be explained by the accumulation of tribo-charges: the saturation of charges on PTFE surface hinders following charge separation upon impact (Fig. S11(b)). Initially, charge accumulation primarily occurs at the point of impact, where tribo-charges steadily accumulate within the contact area. As the surface charge density nears saturation, the weakening of contact electrification leads to water droplets leaving the surface with negligible charges. In high-humidity conditions, tribo-charges also exhibit enduring stability in Fig. S11(c). Moreover, the charged region is influenced by the volume of the water droplet (Fig. S12 in Appendix A).

3.3. Spontaneous transfer mechanism of charges through the droplet

After achieving control over the surface charge density and regions on the PTFE surface through liquid–solid contact electrification, we embarked on investigating the spontaneous deformation mechanism of water droplets on the charged surface in Fig. S13 in Appendix A. A free water droplet of 10 μL was gently deposited onto a pre-charged PTFE surface using an injection pump (Fig. S13(a)). Directly above the droplet, a grounded needle with a diameter of approximately 0.5 mm was fixed, capable of moving up and down through motor control. The overall setup resembled the electric wetting-assisted charge injection technique proposed by Wu et al. [31], with the distinction that they employed droplets as a medium to deposit charges on polymer surfaces, whereas our study involved the removal of surface charges through droplet manipulation, constituting an inverse process. Based on the morphological changes of the droplet, the entire process can be divided into four phases in Fig. 3(a).

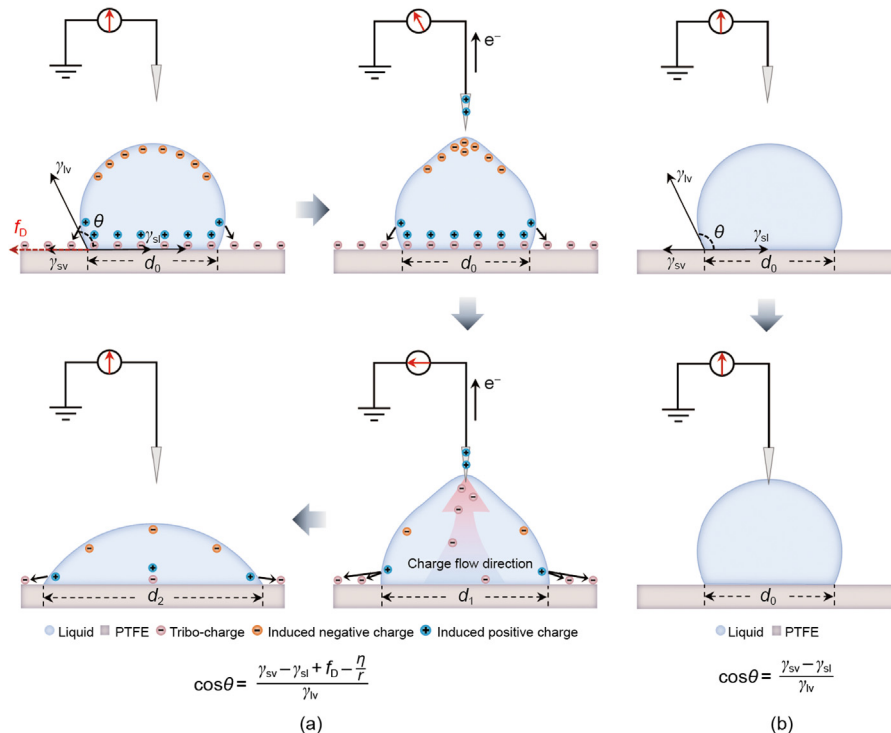


Fig. 3. Mechanism of spontaneous deformation of the water droplet on charged surface. (a) Schematic illustration of the charge distribution change during spontaneous deformation of a droplet on the charged surface. (b) Schematic illustration of the non-deformation of a droplet on an uncharged surface.

As shown in Fig. S13(b), when the grounded needle is positioned at a distance from the droplet, the droplet's presence will influence the electric field distribution within the covered area. From a charge standpoint, as the droplet stabilizes on the charged surface, internal charge stratification occurs due to electrostatic induction. The surface tribo-charges and the induced positive charges attract each other, generating internal tension. Tribo-charges outside the droplet's coverage also induce the generation of polarized charges within the droplet, which enhance the adhesion between the droplet and the surface in the presence of Coulomb force (Fig. S14 in Appendix A). Analyzing using the Young-Laplace equation, when a solid surface carries a charge, the cosine of the contact angle, $\cos\theta$, is influenced by the charges along the three-phase contact line. The balance between the surface tension and the line tension of the three-phase contact line involves only the electrostatic contribution of surface charges. The equation can be expressed as follows [32]:

$$\cos\theta = \frac{\gamma_{sv} - \gamma_{sl} + f_D - \frac{\eta}{r}}{\gamma_{lv}}$$

where γ_{sv} , γ_{sl} , and γ_{lv} represent the surface tension forces of solid-vapor, liquid-solid, and liquid-vapor interfaces, respectively. f_D is the electric driving force of the wetting which denotes the contribution of electrostatic charges. $\frac{\eta}{r}$ represents the electric driving force of line tension contribution.

During the gradual approach of the grounded needle tip toward the top of the droplet, the tip generates positive charges due to electrostatic induction. At this juncture, the mutual Coulombic attraction between the positive and negative charges causes the aggregation of negative charges toward the top of the droplet, leading to an upward protrusion of the droplet in Fig. S13(b). This phenomenon resembles the deflection of a stream of water caused by a charged glass rod brought close to a thin stream of water [33].

Once the needle tip and droplet come into contact, the droplet acts as a conductor and immediately connects the covered charged surface with the ground in Fig. S13(c). The substantial potential difference (> 2 kV) between the charged surface within the droplet's coverage area and the needle tip will drive the negative charges to flow from the PTFE surface toward the ground. Meanwhile, the loss of tribo-charges within the droplet disrupts the force balance between the external, internal, and polarized charges in the boundary region, leading to a drastic deformation of the droplet (Movie S3 in Appendix A). Furthermore, non-uniform charge density distribution can result in spontaneous directional movement of the droplets (Fig. S15 and Movie S4 in Appendix A), which is the underlying principle that achieved self-propelled droplet motion by manipulating charge density gradients [4,20]. Finally, when the potential difference between the charged surface and the needle tip becomes insufficient to drive the remaining charges, the shape of the droplet no longer undergoes changes (Fig. S13(d)). At this point, the contact angle of the droplet significantly reduced (Fig. S16 in Appendix A). For comparison, the droplet on the uncharged surface undergoes no morphological change in the same process in Fig. 3(b).

Subsequently, the mechanism of spontaneous charge transfer was discussed. Similar to the results in Fig. 1(b), an instantaneous charge transfer signal of approximately 40 nC was generated upon the moment when the needle tip contact with the droplet in Fig. 4(a). It was revealed that the charge transfer phase had four distinct nodes, which could potentially be attributed to the rapid and spontaneous deformation of the droplet, resulting in repeated contact and detachment between the droplet and the needle tip. For comparison, in the absence of droplets, the grounded needle tip induces only a minor charges transfer when it approaches the charged surface, because of the lacking of charge conduction

channel (Fig. S17 in Appendix A). Furthermore, significant variations were observed when different liquids were used to transfer tribo-charge on the PTFE surface. As shown in Fig. 4(b), the results indicated that only polar liquids, including water, ethanol, glycerol, and acetonitrile, were capable of transferring surface tribo-charges upon contact with the needle tip. However, differences in the amount of transferred charge may be affected by the inherent properties of liquids, such as surface tension and viscosity [34]. Under identical testing conditions, non-polar liquids such as paraffin, *n*-hexane, and squalane exhibited nearly negligible charge transfer. These findings offer an insight: the phenomenon of spontaneous charge transfer seems to be linked to both the spontaneous electric field and the polarity of the liquid.

Building upon the preceding experimental outcomes, we posit a hypothesis that spontaneous charge transfer on the surface necessitates the simultaneous fulfillment of two key prerequisites: the presence of a strong spontaneous electric field and the polar solvent as an effective charge pathway. Taking water as an illustrative instance, even for DI water, a degree of dissociation occurs, yielding hydronium and hydroxide ions. The electric field will amplify this dissociation, thereby providing a viable path for charge transfer. To support this, Saitta et al. [35] observed notable changes in hydrogen bond lengths and molecular orientation of water under an electric field, alongside a discernible enhancement in the conductivity of water. At the molecular scale, polar solvent molecules tend to align from a disordered configuration to an ordered one under an electric field, facilitating charge transfer via augmented dissociation and proton migration principles. Figs. 4(c)–(e) visually delineate the alterations in electric field distribution and the dissociation–diffusion (D–D) dynamics of water molecules as the grounded needle tip progressively approaches the droplet on charged surface. When the droplet stabilizes on the charged surface, electrostatic induction causes charge separation within its interior, resulting in positive charges at the base and negative charges at the top. Moreover, some tribo-charges are transferred from the surface to the droplet due to conductive electrification [36–38], but the hindering effect of electrostatic induction and the small charge storage potential of the droplet result in an almost negligible amount of transferred charge (Fig. S11) [20,24]. As the needle tip is away from the droplet, the negative charges induced within the droplet and the tribo-charges in the uncovered region combine to create an associated electric field with the needle tip (Fig. 4(c)). Upon the instant contact of the needle tip with the droplet, a fresh electric field of exceeding $2 \text{ kV}\cdot\text{cm}^{-1}$ between the needle tip and the charged surface is established. At this juncture, the spontaneous electric field triggers the dissociation of water molecules, urging the dissociated molecules to reunite with protons migrating from neighboring molecules. This process involves the potential engagement of multiple protons concurrently, which will enhance the charge transmission capacity of water droplet, as depicted in Fig. 4(d). As the depth of contact escalates, the electric field drives the tribo-charges from the PTFE surface to ground through the liquid medium. In this process, due to the rapid decrease in charge density within the covered area of the droplet, the diminished electric field strength can no longer sustain the transfer of surface tribo-charges and the dissociation of water molecules in Fig. 4(e).

Upon applying a negative bias voltage to the needle tip, the transferred charge decreases with increasing voltage due to the reduction in potential difference between the needle tip and the charged surface in Fig. 4(f). Conversely, applying a positive bias voltage to the needle tip enhances the potential difference, leading to a significant increase in the amount of transferred charge. Correspondingly, there is a significant difference in the contact angle of the water droplets after the contact of the needle at different bias voltages (Fig. S18 in Appendix A). Notably, not only is the negative

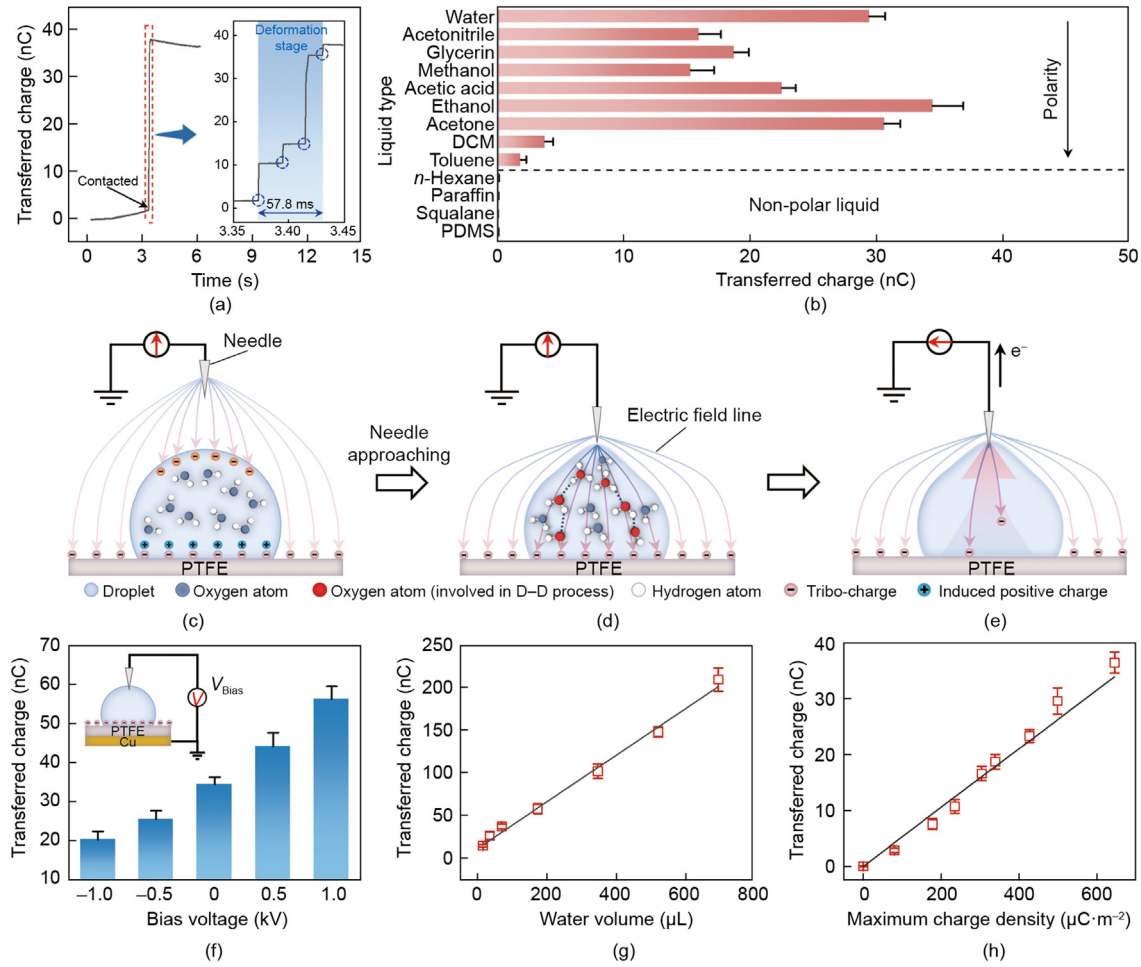


Fig. 4. Mechanism of liquid-induced surface charge transfer. (a) Transferred charge signal when a needle touches the water droplet on a charged surface. (b) Effect of solution type on transferred charge amount. (c)–(e) Schematic illustration of the electric field, charge, and molecular dynamics changes during the approach of the grounding needle tip to the water droplet. (f)–(h) Correlation between (f) transfer charge and bias voltage, (g) water volume, and (h) maximum charge density. Inset: Schematic diagram of the applied bias voltage on the droplet, V_{bias} : bias voltage.

charge entirely transferred, but the reversed electric field direction also induces a local charge-trapping effect [31], leaving positive charges within the covered area of the droplet. Furthermore, the electric field strength is influenced by the distance between the needle tip and charged surface (Fig. S19(a) in Appendix A). As shown in Fig. S19(b), as the needle tip approaches the charged surface, the maximum amount of transferred charge increases with the depth of insertion. The potential distribution on the PTFE surface is also consistent with the charge transfer results in Figs. S19(c) and (d). These results further confirm that the spontaneous electric field between the needle tip and charged surface is the primary driving factor for the transfer of tribo-charges.

Subsequently, the factors influencing the controllable transfer of surface charges were explored. A positive correlation was observed between the transferred charge amount and the droplet volume, owing to the pronounced association between droplet volume and the covered area in Fig. 4(g). Under the consistent surface charge density ($\sim 243 \mu\text{C}\cdot\text{m}^{-2}$), the tribo-charges on different material surfaces could be transmitted through the droplet, despite differences in surface energy leading to variations in the quantities of transferred charge. Moreover, a robust correlation exists between the transferred charge amount and surface charge density in Fig. 4(h), attributed to the heightened surface maximum charge density enhancing the electric field strength. It was observed that the presence of the bottom electrode also affects the induction of

tribo-charges outside the droplet (Fig. S20(a) in Appendix A). There is no significant difference in the surface potential before and after charge transfer whether the tip of the needle is grounded or connected to the bottom electrode (Fig. S20(b) in Appendix A), suggesting that connecting the bottom electrode can be an effective alternative to grounding. Similarly, tribo-charges generated on the PTFE surface through solid–solid friction or air ionization can be transferred using the same approach (Fig. S21 in Appendix A), and the polarity of the charges does not influence the effectiveness of charge transfer (Fig. S22 in Appendix A). Additionally, surface charge transfer within a specific region can be achieved by varying the area covered by the droplet (Fig. S23 in Appendix A).

3.4. Dual-electrode DD-TENG

We demonstrated the feasibility of continuous contact electrification and charge transfer using a single water droplet (Fig. S24(a) in Appendix A). Moreover, a higher release height of the droplet led to a larger quantity of transferred charge in Fig. S24(b), with the potential at the center notably lower than at the periphery in Fig. S24(c). Based on this, we designed a DD-TENG that combines processes of contact electrification and water droplet-induced charge transfer, which can significantly improve the efficiency of tribo-charge utilization in Fig. 5(a). The DD-TENG comprises a bottom electrode, a PTFE film, and a top electrode, with the top elec-

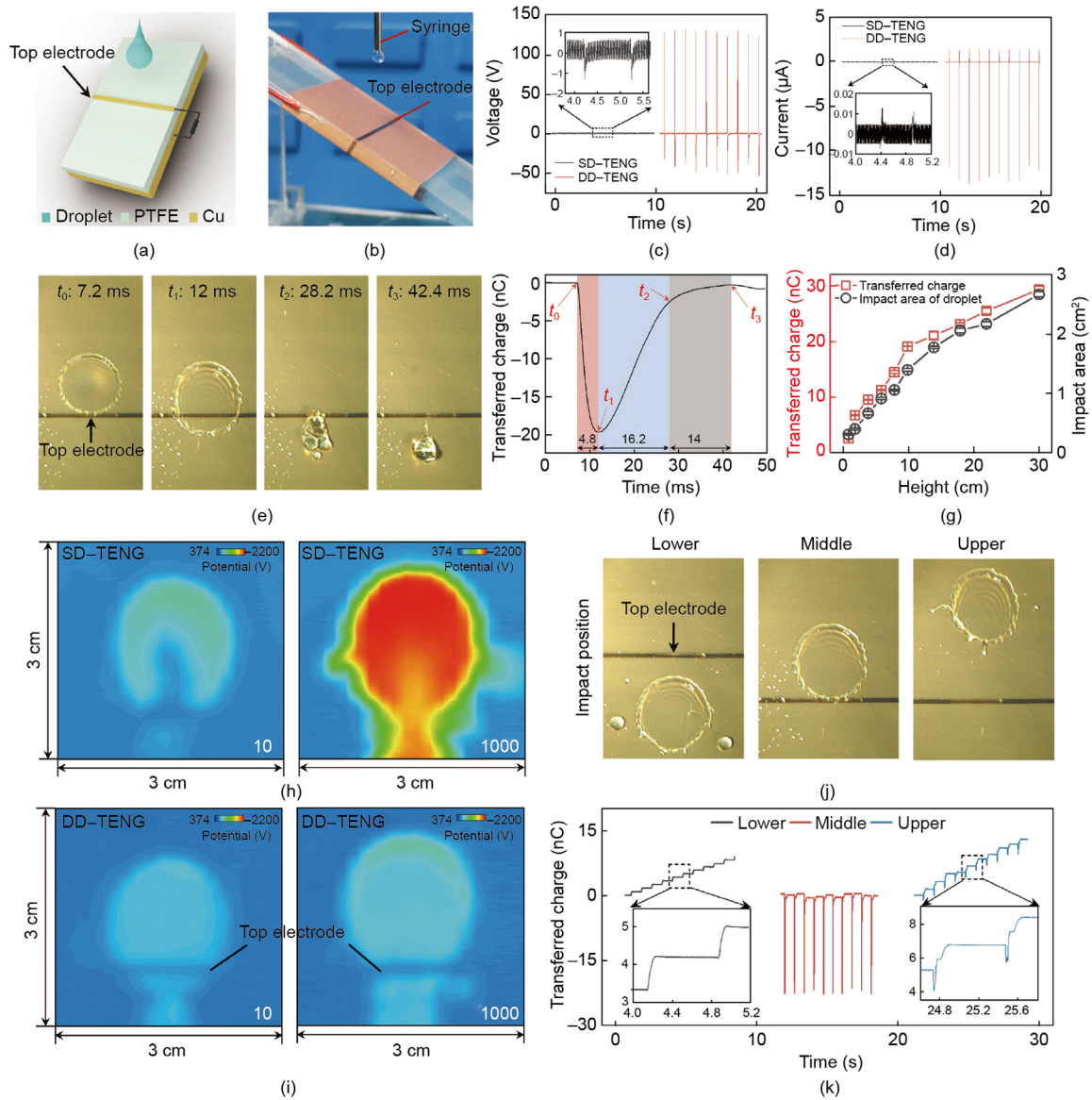


Fig. 5. Efficiency boost of droplet energy harvesting realized by water-induced tribo-charge transfer. (a) Schematic diagram of the DD-TENG structure. (b) A photograph of the DD-TENG. (c) Output voltage of DD-TENG and SD-TENG. (d) Output current of DD-TENG and SD-TENG. (e) Morphology changes of the water droplet impacting the DD-TENG surface and corresponding time points. (f) Transferred charge signal and time span during the droplet impact. (g) Effect of dripping height on transfer charge amount and impact area. (h, i) Surface potential distribution of (h) SD-TENG and (i) DD-TENG after different number of working cycles. (j) Impact points of the droplet. (k) Effect of impact position on transfer charge signal of DD-TENG.

trode connected to the bottom electrode through an external load during testing in Fig. 5(b). During operation, the impact of the water droplet on the top electrode generates alternating current (AC) signals. A small droplet of 35 μL is sufficient to drive the DD-TENG and produce an open-circuit voltage of approximately 125 V, a short-circuit current of 13 μA , and a transferred charge of 20 nC (Figs. 5(c) and (d), and Fig. S25(a) in Appendix A). Under the same testing conditions, the conventional SD-TENG can only output 1.4 V, 0.01 μA , and 0.05 nC, respectively, significantly lower than the DD-TENG. Additionally, the DD-TENG can easily illuminate about 52 series-connected LEDs in Fig. S25(b).

The morphology of water droplets and the corresponding signal during the operation of the DD-TENG were also investigated. As depicted in Fig. 5(e) and Movie S5 in Appendix A, the deformation process of water droplet impact on the device surface was captured at four time points. The entire deformation process takes about 35 ms, and the change in the transferred charge signal over time was

recorded simultaneously. As shown in Fig. 5(f), with the signal rising from the onset to the peak within about 4.8 ms, and then descending from the peak to the end over a span of about 30.2 ms. The deformation of the droplet aligns perfectly with the regularity of the charge signal. The DD-TENG was also flatly placed to confirm whether the change in area during water droplet contact matched the signal pattern (Fig. S26 in Appendix A).

We further investigate the output enhancement mechanism of DD-TENG compared to SD-TENG. Figs. 5(h) and (i) illustrates the surface potential evolution of SD-TENG and DD-TENG structures after different numbers of working cycles. For the SD-TENG, the surface potential reaches approximately -2144 V after 1000 working cycles (i.e., water droplet impact events), indicating a continuous accumulation of surface charges. In contrast, the DD-TENG exhibits only a slight increase. There are also differences in the charge quantities carried by water droplets after impact on the two device surfaces. The methods used to quantify the carried

charge by water droplets upon impact on both device types are presented in Fig. S27(a) and (b) (Appendix A). The results reveal a gap of approximately 30-fold in carried charge quantities by water droplets impacting the two device surfaces in Fig. S27(c). It can be inferred that the presence of the upper electrode in the DD-TENG impedes the continuous accumulation of surface tribo-charges. This result is possibly attributed to the upper electrode's role in serving as the "ground needle," allowing water droplets to act as pathways for the transmission of surface tribo-charges. Furthermore, differences are observed in the initial state of the transferred charge signals between the two TENGs (Fig. S28 in Appendix A). These outcomes indicate that the output of the DD-TENG is not solely dependent on the induction of surface charges. To demonstrate the role of the upper electrode in facilitating surface tribo-charge transmission, an experiment involving the injection of charges onto the DD-TENG surface prior to studying charge transfer behavior upon water droplet impact was conducted. The results reveal similar characteristics, where the first water droplet impact event induces significantly higher transferred charge amount (Fig. S29 in Appendix A), suggesting it can induce the transmission of surface charges injected in advance. This observation aligns with the DD-TENG surface potential depicted in Fig. 5(i), indicating that the overall charge transfer process involves not only the transmission of surface charges but also the induction of "trapped charges."

To further investigate the working mechanism of DD-TENG, the effect of droplet impact position was investigated in Fig. 5(j). As depicted in Fig. 5(k), when the impact point is below the upper electrode, the characteristics of the charge transfer signal align with those of the initial stage of SD-TENG, given that the tribo-charge in the impact region cannot transmit through the upper electrode. When the impact point is on the upper electrode, the amount of charge transfer is maximal. In cases where the impact

point is above the upper electrode, the charge signal includes both a step signal and an AC signal. This phenomenon can be elucidated by the fact that during the impact process, contact electrification results in the generation of tribo-negative charges in the impact region, accompanied by an equivalent amount of positive charges within the droplet. As the droplet shrinks due to gravity and slides over the upper electrode, charge transfer and electrostatic induction occur, generating an AC signal. When the droplet completely detaches from the surface, the tribo-charges in the impact region remain unshielded, resulting in an induced step signal.

Based on the aforementioned experimental observations and results, the operating principle of DD-TENG can be summarized as the coupling of contact electrification, water-induced charge transfer, and electrostatic induction. As illustrated in Fig. 6(a), when the DD-TENG is in a stable state, "trapped charges" on PTFE surface are saturated, while the bottom electrode induces an equivalent positive charge. Upon water droplet impact on the surface and subsequent spreading, due to contact electrification, negative and positive tribo-charges are generated on the PTFE surface and droplet, respectively. When the spreading droplet contacts the upper electrode, the water droplet will induce the new tribo-charges on the PTFE surface transfer to the bottom electrode, until establishing a new charge balance. Subsequently, as the water droplet starts to shrink due to gravity and surface tension, the contact area between the water droplet and the surface diminishes. Since the surface trapped charges are not screened by the positive charges in the water droplet, a potential difference emerges, which drives the positive charges to flow from the water droplet to the bottom electrode to equalize the trapped charges. This process continues until the water droplet detaches from the PTFE surface. It's important to note that when the impact point of the water droplet is on the upper electrode, the mechanism slightly differs, with

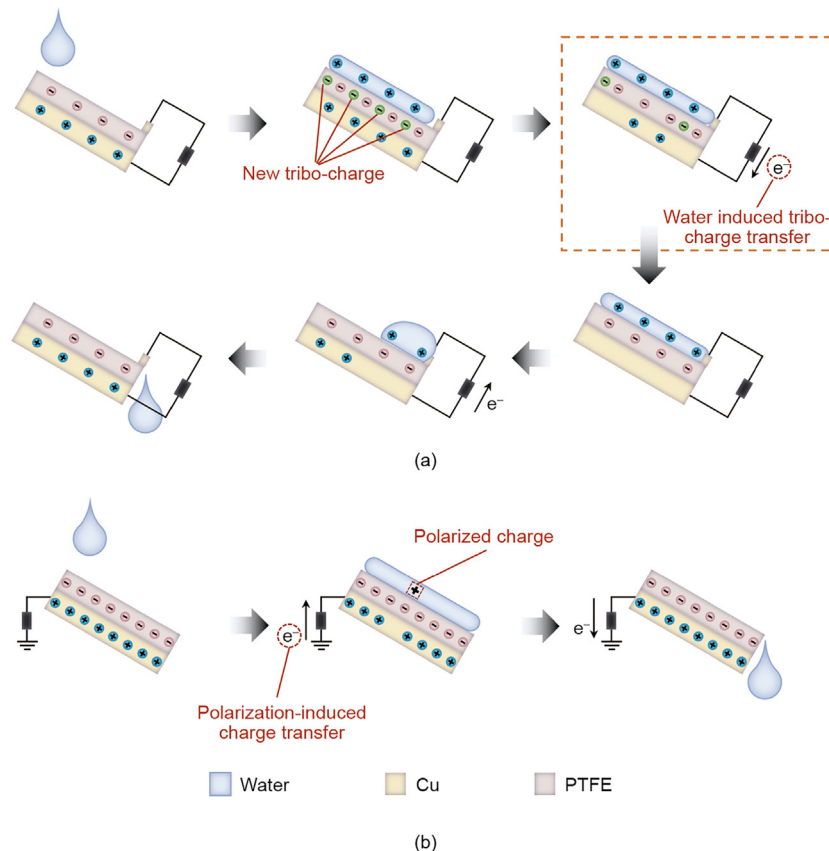


Fig. 6. Difference between DD-TENG and SD-TENG in working principle. Schematic diagram of charge transfer process during operation of (a) DD-TENG and (b) SD-TENG.

tribo-charge generation and charge transmission possibly occurring simultaneously, although the influence on the quantity of transferred charge is not significant. Comparatively, the output performance of the SD-TENG is much lower in Fig. 6(b). In a stable state, the surface tribo-charges of the SD-TENG are already saturated, rendering subsequent water droplet impacts unable to generate new surface charges. Its output depends on the polarized charge in the water droplet, which is much less than the new tribo-charges generated during the operation of the DD-TENG. In summary, the DD-TENG realizes the dynamic manipulation of liquid–solid tribo-charge through the water droplet-induced charge transfer to improve the efficiency of water-related energy harvesting.

We subsequently investigated the key parameters that affect the output of DD-TENG. First, the effective area significantly impacts the DD-TENG's output. As shown in Fig. 5(g) and Figs. S30–S33 in Appendix A, factors such as droplet falling height, droplet volume, flow velocity, and impact angle affect the actual contact area of the droplet, thereby exerting a substantial influence on the DD-TENG's output. Furthermore, there exists an inverse correlation between the width of the upper electrode and the actual electrified area (Fig. S34 in Appendix A). The type and thickness of the contact material respectively affect the contact electrification and electrostatic induction processes, thus playing a vital role in the DD-TENG's output (Fig. S35 in Appendix A). The nature of water droplets also has an impact on the output performance of the DD-TENG. As shown in Fig. S36(a) in Appendix A, the transfer charge quantity of DD-TENG exhibits a trend of initial plateau followed by a decrease with increasing NaCl concentration in the solution. Notably, when driven by rainwater or tap water, the transfer charge quantity and current of DD-TENG do not exhibit significant decreases in Fig. S36(b).

Moreover, the DD-TENG demonstrates excellent resistance to extreme environments, reproducibility, and long-term stability (Figs. S37 and S38 in Appendix A). Concurrently, when using deionized water to drive the DD-TENG, both the instantaneous output power density and highest conversion efficiency of the DD-TENG exceeded $1 \text{ W} \cdot \text{m}^{-2}$ and 1.2%, as depicted in Fig. S39 (Appendix A). At a NaCl concentration of 0.01 mol L^{-1} , the DD-TENG achieves a peak power density of $\sim 1 \text{ W} \cdot \text{m}^{-2}$, yielding an energy of $0.6 \mu\text{J}$ per droplet of $35 \mu\text{L}$ (Figs. S40(a) and (b) in Appendix A). Notably, under simulated scenarios using tap water and rainwater, the DD-TENG maintains a robust output, highlighting its potential for practical applications (Figs. S40(c) and (d) in Appendix A).

4. Conclusions

In conclusion, based on the manipulation of liquid–solid contact to achieve controllable charged surface construction, we propose a strategy for water droplet-induced directional transport of tribo-charges (mostly electrons) and accompanying energy harvesting. Unlike previous work that focused on the exploitation of the static properties of electrostatic charges, the discovery of dynamic water droplet-induced tribo-charge transport mechanism greatly enriches our ability to control and utilize charges. In addition, the DD-TENG developed based on this mechanism also achieves a new breakthrough in the efficiency of water-related energy harvesting. From a broader perspective, the generalization of our approach will open up new avenues for a wide range of applications, ranging from physics to energy and sensing technologies.

Acknowledgments

Research was supported by the Natural Science Foundation of Zhejiang Province (LZ22C130001), the National Natural Science

Foundation of China (32171887, and 52002028, and 52192610), the National Key Research and Development Project from Minister of Science & Technology (2021YFA0202704), and Beijing Municipal Science & Technology Commission (Z171100002017017).

Appendix A. Supplementary data

Supplementary data to this article can be found online at <https://doi.org/10.1016/j.eng.2024.07.013>.

References

- [1] McCarty LS, Whitesides GM. Electrostatic charging due to separation of ions at interfaces: contact electrification of ionic electrets. *Angew Chem Int Ed* 2008;47(12):2188–207.
- [2] Averin DV, Nazarov YV. Virtual electron diffusion during quantum tunneling of the electric charge. *Phys Rev Lett* 1990;65(19):2446–9.
- [3] Lee JK, Han HS, Chaikasetsin S, Marron DP, Waymouth RM, Prinz FB, et al. Condensing water vapor to droplets generates hydrogen peroxide. *Proc Natl Acad Sci USA* 2020;117(49):30934–41.
- [4] Li X, Bista P, Stetten AZ, Bonart H, Schür MT, Hardt S, et al. Spontaneous charging affects the motion of sliding drops. *Nat Phys* 2022;18(6):713–9.
- [5] Barringer SA, Sumonsiri N. Electrostatic coating technologies for food processing. *Annu Rev Food Sci Technol* 2015;6(1):157–69.
- [6] Prasad LK, McGinity JW, Williams III RO. Electrostatic powder coating: principles and pharmaceutical applications. *Int J Pharm* 2016;505:289–302.
- [7] Pel J, Broemeling D, Mai L, Poon HL, Tropini G, Warren RL, et al. Nonlinear electrophoretic response yields a unique parameter for separation of biomolecules. *Proc Natl Acad Sci USA* 2009;106(35):14796–801.
- [8] Saucedo-Espinosa MA, Ditttrich PS. In-droplet electrophoretic separation and enrichment of biomolecules. *Anal Chem* 2020;92(12):8414–21.
- [9] Wang ZL. Triboelectric nanogenerators as new energy technology for self-powered systems and as active mechanical and chemical sensors. *ACS Nano* 2013;7(11):9533–57.
- [10] Cheng T, Shao J, Wang ZL. Triboelectric nanogenerators. *Nat Rev Methods Primers* 2023;3(1):39.
- [11] Lin ZH, Cheng G, Lee S, Pradel KC, Wang ZL. Harvesting water drop energy by a sequential contact-electrification and electrostatic-induction process. *Adv Mater* 2014;26(27):4690–6.
- [12] Zhu G, Su Y, Bai P, Chen J, Jing Q, Yang W, et al. Harvesting water wave energy by asymmetric screening of electrostatic charges on a nanostructured hydrophobic thin-film surface. *ACS Nano* 2014;8(6):6031–7.
- [13] Lin ZH, Cheng G, Lin L, Lee S, Wang ZL. Water–solid surface contact electrification and its use for harvesting liquid-wave energy. *Angew Chem Int Ed* 2013;52(48):12545–9.
- [14] Levin Z, Hobbs PV. Splashing of water drops on solid and wetted surfaces: hydrodynamics and charge separation. *Philos T R Soc A* 1971;269(1200):555–85.
- [15] Skinner LB, Benmore CJ, Shyam B, Weber JKR, Parise JB. Structure of the floating water bridge and water in an electric field. *Proc Natl Acad Sci USA* 2012;109(41):16463–8.
- [16] Fuchs EC, Woisetschläger J, Gatterer K, Maier E, Pecnik R, Holler G, et al. The floating water bridge. *J Phys D Appl Phys* 2007;40(19):6112.
- [17] Hosono T, Kato K, Morita A, Okubo H. Surface charges on alumina in vacuum with varying surface roughness and electric field distribution. *IEEE Trans Dielectr Electr Insul* 2007;14(3):627–33.
- [18] Quinn A, Sedev R, Ralston J. Contact angle saturation in electrowetting. *J Phys Chem B* 2005;109(13):6268–75.
- [19] Ali HAA, Mohamed HA, Abdelgawad M. Repulsion-based model for contact angle saturation in electrowetting. *Biomechanics* 2015;9(1):014115.
- [20] Sun Q, Wang D, Li Y, Zhang J, Ye S, Cui J, et al. Surface charge printing for programmed droplet transport. *Nat Mater* 2019;18(9):936–41.
- [21] Chun J, Ye BU, Lee JW, Choi D, Kang CY, Kim SW, et al. Boosted output performance of triboelectric nanogenerator via electric double layer effect. *Nat Commun* 2016;7(1):12985.
- [22] Tang Z, Yang D, Guo H, Lin S, Wang ZL. Spontaneous wetting induced by contact-electrification at liquid–solid interface. *Adv Mater* 2024;36(25):2400451.
- [23] Lin S, Chen X, Wang ZL. Contact electrification at the liquid–solid interface. *Chem Rev* 2022;122(5):5209–32.
- [24] Zhan F, Wang AC, Xu L, Lin S, Shao J, Chen X, et al. Electron transfer as a liquid droplet contacting a polymer surface. *ACS Nano* 2020;14(12):17565–73.
- [25] Wang ZL, Wang AC. On the origin of contact-electrification. *Mater Today* 2019;30:34–51.
- [26] Nie J, Ren Z, Xu L, Lin S, Zhan F, Chen X, et al. Probing contact-electrification-induced electron and ion transfers at a liquid–solid interface. *Adv Mater* 2020;32(2):1905696.
- [27] Lin S, Xu L, Chi Wang A, Wang ZL. Quantifying electron-transfer in liquid–solid contact electrification and the formation of electric double-layer. *Nat Commun* 2020;11(1):399.

- [28] Li S, Nie J, Shi Y, Tao X, Wang F, Tian J, et al. Contributions of different functional groups to contact electrification of polymers. *Adv Mater* 2020;32(25):2001307.
- [29] Sun M, Lu Q, Wang ZL, Huang B. Understanding contact electrification at liquid–solid interfaces from surface electronic structure. *Nat Commun* 2021;12(1):1752.
- [30] Hang L, Li X, Zhang Y, Feng Y, Zhou F, Wang D. Regulation and influence factors of triboelectricity at the solid–liquid interface. *Nano Energy* 2020;78:105370.
- [31] Wu H, Mendel N, van der Ham S, Shui L, Zhou G, Mugele F. Charge trapping-based electricity generator (CTEG): an ultrarobust and high efficiency nanogenerator for energy harvesting from water droplets. *Adv Mater* 2020;32(33):2001699.
- [32] Digilov R. Charge-induced modification of contact angle: the secondary electrocapillary effect. *Langmuir* 2000;16(16):6719–23.
- [33] Woisetschlager J, Wexler AD, Holler G, Eisenhut M, Gatterer K, Fuchs EC. Horizontal bridges in polar dielectric liquids. *Exp Fluids* 2012;52(1):193–205.
- [34] Jin Y, Xu W, Zhang H, Li R, Sun J, Yang S, et al. Electrostatic tweezer for droplet manipulation. *Proc Natl Acad Sci USA* 2022;119(2):e2105459119.
- [35] Saitta AM, Saija F, Giaquinta PV. *Ab initio* molecular dynamics study of dissociation of water under an electric field. *Phys Rev Lett* 2012;108(20):207801.
- [36] Sun Y, Huang X, Soh S. Solid-to-liquid charge transfer for generating droplets with tunable charge. *Angew Chem Int Ed* 2016;55(34):9956–60.
- [37] Jin Y, Liu X, Xu W, Sun P, Huang S, Yang S, et al. Charge-powered electroaxis for versatile droplet manipulation. *ACS Nano* 2023;17(11):10713–20.
- [38] Jin Y, Wu C, Sun P, Wang M, Cui M, Zhang C, et al. Electrification of water: from basics to applications. *Droplet* 2022;1(2):92–109.